PAPER

Transition path properties for one-dimensional non-Markovian models

IOP Publishing Journal of Physics A: Mathematical and Theoretical
J. Phys. A: Math. Theor. **57** (2024) 355201 (25pp) https://doi.org/10.1088/1751-8121/ad6db1

Transition path properties for one-dimensional non-Markovian models

Hua Li[1], **Yong Xu**[2,3,*], **Ralf Metzler**[4,5] **and Jianwei Shen**[1]

[1] School of Mathematics and Statistics, North China University of Water Resources and Electric Power, Zhengzhou 450046, People's Republic of China
[2] Department of Applied Mathematics, Northwestern Polytechnical University, Xi'an 710072, People's Republic of China
[3] MOE Key Laboratory for Complexity Science in Aerospace, Northwestern Polytechnical University, Xi'an, 710072, People's Republic of China
[4] Institute for Physics & Astronomy, University of Potsdam, 14476 Potsdam-Golm, Germany
[5] Asia Pacific Center for Theoretical Physics, Pohang 37673, Republic of Korea

E-mail: hsux3@nwpu.edu.cn

Received 21 May 2024; revised 31 July 2024
Accepted for publication 9 August 2024
Published 21 August 2024

Abstract

Transitions between long-lived states are rare but important. The statistic of successful transitions is considered in transition path theory. We here consider the transition path properties of a generalized Langevin equation with built-in memory. The general form of the approximate theoretical solutions to the transition path time distribution, mean transition path time, and coefficient of variation are obtained from the generalized Smoluchowski equation. Then, the accuracy of our theoretical results is verified by the Forward Fluxing Sampling scheme. Finally, two examples are worked out in detail. We quantify how the potential function and the memory parameters affect the transition path properties. The short time limit of transition path time distribution always has an exponential decay. For the parabolic potential case, the memory strongly affects the long-time behavior of the transition path time distribution. Our results show that the behavior of the mean transition path time is dominated by the smaller of the two memory times when both memory times exceed the intrinsic diffusion time. Interestingly, the results also show that the memory

* Author to whom any correspondence should be addressed.

can effect a coefficient of variation of transition path times exceeding unity, in contrast to Markovian case.

Keywords: transition path properties, generalized Langevin equation, transition path time, transition path time distribution, memory

1. Introduction

Random disturbances inevitably exist in various systems, inducing various stochastic dynamic phenomena, such as early warning concepts in high-amplitude noise-induced oscillations [1], stochastic bifurcations [2], coherence resonance [3], tipping delay [4], and the exit problem [5], to name but a few. Specifically, the phenomenon of the noise-driven exit problem has gained increasing attention. The original treatment of thermal noise-driven escape from a potential well was due to Kramers [6]. There, in the small-noise or high-potential barrier limit, the waiting time of particles near a stable state is quite long, while the exit process is completed (comparatively) instantaneously. In other words, this process is an exit problem with a rather small probability, a rare event [7, 8]. Transition path theory, instead, considers only the successful, fast trajectories across the barrier [9–11]. In general, given a region (x_A, x_B), a 'transition path' trajectory connects the initial point at the bottom of the well to the final point across the barrier, without revisits to the transition region.

The transition path [9–11] contains the key information of the exit problem, capturing the rare escape events. It is vital in protein configuration analysis, engineering safety design, clinical drug development, inter alia [12]. The transition path time (TPT) [13, 14] is the duration of the transition path, which describes the time spent during the exit dynamics. Usually, the TPT is considerably shorter than the exit time (the inverse of the Kramers rate). The transition path time distribution (TPTD) [15, 16] is a specific measure for the transition path properties. The width of the transition and exit time distributions contains vital information about the dynamic of the system. Thus, the short-time behavior of first-exit distributions reveal information about kinetic intermediates [17]. In turn, long time tails of TPTD indicate the possible existence of a trap in the transition path region [18]. In the case of escape of particles across a potential barrier, the width of the TPTD of a higher potential barrier cannot be broader than a single-exponential [19]. The coefficient of variation (COV) is applied to quantify the width of a distribution and is used in various fields from engineering to economics. The value of the COV is small for narrower distributions, while a heavy-tailed distribution has a COV exceeding unity, and the variation coefficient of an exponential distribution equals unity [20]. Moreover, the COV of a TPTD reveals the dimensionality of the underlying free energy landscape. A coefficient of variation exceeding unity is also a characteristic of multidimensional dynamics [19, 21].

Interestingly, there exists a series of results concerning the transition path behavior of one-dimensional Markovian systems. Since the solution and analysis of transition path properties involve the solution of the Fokker–Planck-Kolomgorov equation (forward and backward) of the system [22, 23], the corresponding research work is mainly carried out on the transition path of one-dimensional systems from numerical methods points of view, the establishment of basic transition path theory [24, 25], the exploration of approximate theoretical methods, and the analysis of noise mechanism, etc. Generally, it is necessary to extract the statistical data of the transition path according to the sampling of rare events [26]. In the small-noise or high-potential barrier limit, rare events have the characteristics of long waiting times and short durations, resulting in a short duration of the transition path itself, which is thus difficult to capture [27]. Therefore, a series of simulation algorithms are proposed, such as the transition

interface sampling method [28], the umbrella sampling scheme [29], or the string method [30], which are suitable for equilibrium steady-state systems. The Forward Flux Sampling (FFS) method [31, 32] is proposed to realize simulations of rare events in the non-equilibrium case. Subsequently, the FFS scheme was also extended to one-dimensional Markovian system under Gaussian colored noise [7]. In recent years, neural network algorithms for the prediction of stochastic dynamical systems and the capture of dynamical behavior are flourishing [33–36]. Neural network algorithms enable accelerated sampling of system transition paths, which is an additional tool for numerical studies of system transition path dynamics [37].

The theoretical calculation of transition path properties can be reduced to the solution of second-order partial differential equations with two absorbing boundary condition [38]. However, the types of partial differential equations that can be solved by approximate theory are quite limited [39]. Much work has been devoted to this issue for transition path properties. The basis for theoretical calculations of the transition path properties of one-dimensional diffusion systems is presented in [9, 10]. One-dimensional diffusive systems that can provide approximate theoretical results of transition path properties are quite diverse. For instance, the approximate theoretical form of transition path properties of a tip barrier, conical tube, over-damping cases and rough potentials were considered [40–42]. Many interesting transition path properties are beginning to emerge. The transition path properties of equilibrium systems exhibit forward and backward symmetry [43]. Surprisingly, some noisy and non-equilibrium systems may result in the breakdown of transition path properties symmetry, such as dichotomous, Lévy-stable, and Poisson white noises [44–46]. The COV obtained from the TPTD cannot possibly exceed unity for any one-dimensional diffusive model with an arbitrary potential [21], whereas for the trapping site model, it may exceed unity [47]. We mention that all the above studies are based on the transition path properties based on the Langevin equation.

Actually, the Langevin equation can only portrays Brownian motion, and it is a critical problem to describe the many stochastic processes in nature that exhibit anomalous diffusion phenomena. Considering the viscoelasticity of many systems and the memory of their friction, the generalized Langevin equation (GLE) [48] was generalized to an integral form with a friction memory kernel to obtain the generalized Langevin equation that can characterize anomalous diffusion phenomena [49]. In particular, the friction term in GLE is determined by the time-varying memory kernel [50], and the common friction memory kernels are power-law memory [51, 52], tempered memory [53], positive Prony memory [54, 55], bi-exponential memory [56] and other special forms [57]. It has been revealed that the GLE with friction memory kernel can generate many special and complex dynamical behaviors of stochastic dynamic systems. Changes due to GLE with friction memory kernel include escape behavior [58], stochastic resonance [59], anomalous behavior [60, 61], ergodicity [62, 63] and special transition path properties. A consistent description of protein-folding dynamics must account for memory of GLE friction effects [64], and memory effects in the friction significantly speed up peptide folding and unfolding kinetics [65]. The lower barriers result in broader distributions of TPT for GLE with a power-law-type memory kernel [66], memory can lead to a decrease in the TPT [67]. Meanwhile, it also strongly affect the short time behavior of TPT distribution [68]. Usually, coefficient variation of TPT distribution is small than 1 for GLE with exponential memory [19, 69], but whether the same conclusion holds for more complicated memory kernels in an open question [20, 21]. Therefore, considering the special properties of the GLE with memory, this article is concerned with the transition path behaviors of GLE with more complicated memory which has a form of a finite Prony series. However, as memory kernels become more complex, it may lead to an increase in the dimensionality of the system, thus the theoretical solution of the transition path properties will face great challenges, while numerical simulation will be also rather time-consuming. In this paper, we focus on the theoretical

portrayal of the transition path dynamics of the generalized Langevin equation with built-in memory. Therefore, for the numerical study of the transiton path properties of this system, we choose the efficient FFS algorithm with which we are more familiar.

The remainder of this paper is organized as follows. In section 2, the associated approximate description based the generalized Smoluchowski equation is presented. Subsequently, section 3 illustrates the simulation technique used to verify the approximate solution of the TPTD and the mean TPT. The specific derivation of the approximate solution of the TPTD, mean TPT and variation coefficient for two prototypical examples are unfolded in section 4. Then, section 5 the approximate approach are applied to two examples in detail, from which the application and effectiveness of the approximate theoretical solution of transition path properties are demonstrated. The results and perspectives are discussed in section 6.

2. Transition path time and coefficient of variation

Extending the friction term of the standard Langevin equation to a non-local formulation in time with a memory kernel, we obtain the generalized Langevin equation [70, 71]. Depending on the kernel of this equation, this model includes the description of anomalous diffusion phenomena. In this spirit we consider a one-dimensional differential equation with memory kernel, based on the generalized Langevin equation

$$m\ddot{x}(t)+\int_0^t \xi(t-t')\,\dot{x}(t')\,\mathrm{d}t'+f(x)=\epsilon(t)\,, \tag{1}$$

where $x(t)$ is the time dependent reaction coordinate, m is the effective mass of $x(t)$, and $\dot{x}(t)$, $\ddot{x}(t)$ are the first and second order derivatives with respect to time t, respectively. The force is $f(x)=-\mathrm{d}U(x)/\mathrm{d}x$ in terms of the external potential $U(x)$, where we mainly focus on two basic potentials shown in figure 1, namely, the parabolic and inverted parabolic potential $U(x)=\pm kx^2/2$ with force constant $k>0$. We define the transition region of particle as $(x_A,x_B)=(-1,1)$. Such reaction coordinates could be the relative distance between two aminoacids in a protein [72] or the number of monomers of a polymer already translocated through a pore in a membrane [73]. We assume that the stochastic force $\epsilon(t)$ in equation (1) has zero mean, $\langle\epsilon(t)\rangle=0$ and fulfils the second fluctuation-dissipation relation $\langle\epsilon(t)\epsilon(s)\rangle=k_BT\xi(|t-s|)$ with the friction kernel, where $\langle\cdot\rangle$ denotes an ensemble average (average over realizations). Moreover, k_B is the Boltzmann constant and T is the absolute temperature of the environment. The system is therefore at equilibrium.

We consider equation (1) with a memory kernel of the form of a finite Prony series [74, 75], i.e.

$$\xi(t)=2\alpha_0\delta(t)+\frac{\alpha_1}{\tau_1}\exp\left(-\frac{t}{\tau_1}\right)+\frac{\alpha_2}{\tau_2}\exp\left(-\frac{t}{\tau_2}\right), \tag{2}$$

where $\delta(t)$ is the Dirac delta function, τ_1 and τ_2 are two memory time scales, and α_1 and α_2 are the corresponding friction coefficients. Specifically, if $\alpha_0=0$, $\epsilon(t)$ reduces to thermal band-passing colored noise [56]. We define $\alpha=\alpha_1+\alpha_2$ as the total friction coefficient. For the subsequent discussion of the effect of the two memory time scales τ_1 and τ_2 on the transition path properties, we introduce the intrinsic time scales [76],

$$\tau_m=\frac{m}{\alpha},\quad \tau_D=\beta x_B^2\alpha, \tag{3}$$

where we call τ_m the inertial time and τ_D is the intrinsic diffusion time.

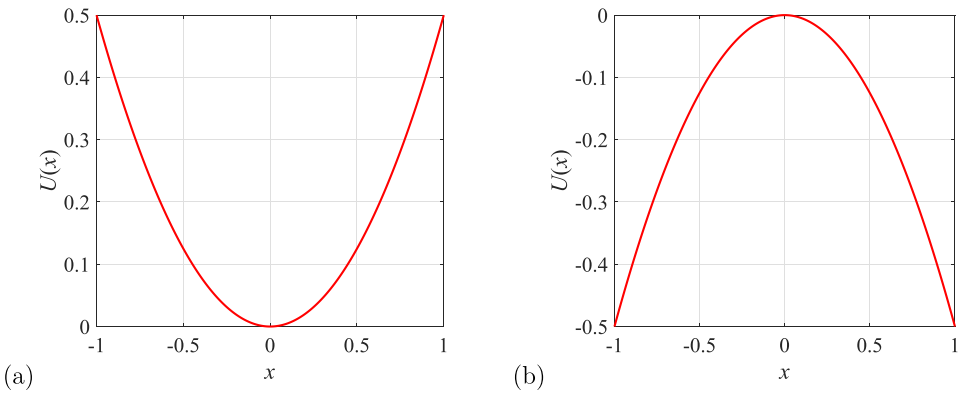

Figure 1. External parabolic and inverted parabolic potentials $U(x)$ considered in this article. (a) $U(x) = kx^2/2$, (b) $U(x) = -kx^2/2$ for $k > 0$.

In the approach chosen in this work, we neglect inertial effects in the stochastic differential equation (1) and consider the 'overdamped' generalized Langevin equation

$$-f(x) = -\int_0^t \xi(t-t')\,\dot{x}(t')\,\mathrm{d}t' + \epsilon(t)\,. \tag{4}$$

We will consider the transition path properties of this stochastic differential equation.

2.1. Transition path time distribution

We first study the distribution of TPTs with the transition region (x_A, x_B), where $x_A = -1$ and $x_B = 1$ are two absorbing boundaries. To determine the TPT distribution, we consider the Green's function of equation (4), which satisfies the following 'generalized Smoluchowski equation' (GSE) [77]

$$\frac{\partial P(x,t|x_0,0)}{\partial t} = D(t)\,\frac{\partial}{\partial x}\left(-\beta f(x) + \frac{\partial}{\partial x}\right) P(x,t|x_0,0)\,, \tag{5}$$

where $P(x,t|x_0,0)$ is the conditional probability that a particle is located at x at time instance t, given that it was released at x_0 at the initial time $t = 0$, i.e. $P(x,t|x_0,0)$ is the solution of equation (5) for the initial condition $P(x,t|x_0,0) = \delta(x - x_0)$, given the absorbing boundary conditions $P(x_A,t|x_0,0) = P(x_B,t|x_0,0) = 0$. $\beta = 1/k_BT$ is the Boltzmann coefficient, and $D(t)$ is a time-dependent diffusion coefficient to be specified. $D(t)$ is given by [78]

$$D(t) = -\langle x^2(0)\rangle \frac{\mathrm{d}}{\mathrm{d}t}\left(\log\left[\Lambda(t)\right]\right), \tag{6}$$

where $\Lambda(t)$ is the so-called normalized reaction coordinate, $\Lambda(t) = \langle x(t)x(0)\rangle / \langle x^2(0)\rangle$. We note that the GSE (5) is only an approximation, time-dependent coefficients cannot fully replace correaltions in the GLE, the real process described by such effective diffusion equations is actually scaled Brownian motion, in which the Langevin equation is characterised by $D(t) \propto t^{\alpha_3 - 1}$ (mean squared displacement $\langle x^2(t)\rangle \sim 2K_{\alpha_3} t^{\alpha_3}$, K_{α_3} is anomalous diffusion coefficient). However, we will show from stochastic simulations that it provides a rather good description

of the process. Generally, non-Markovian processes cannot be completely characterized by corresponding Fokker–Planck equations while the process is completely characterized in terms of the generalized Langevin equation [79, 80].

The TPTD $\rho(t)$ is proportional to the flux of trajectories and specifically defined via [42]

$$\rho(t) = \lim_{\theta\to 0} \frac{q(x_B, t|x_A+\theta, 0)}{\int_0^\infty q(x_B, t|x_A+\theta, 0)\,\mathrm{d}t}, \tag{7}$$

where $\pi_B(x_A) = \int_0^\infty q(x_B, t|x_A, 0)\mathrm{d}t$ is the so-called splitting probability [42]. Moreover, $q(x_B, t|x_A, 0)$ is the flux from x_A to x_B, that follows

$$q(x_B, t|x_A, 0) = -D(t)\left(-\beta f(x) + \frac{\partial}{\partial x}\right) P(x, t|x_A, 0)\Big|_{x=x_B}. \tag{8}$$

Finally, the TPTD $\rho(t)$ of the particles in the transition region from point x_A to x_B can be obtained from the flux $q(x, t|x_0, 0)$ near the point x_B,

$$\rho(t) = \frac{q(x_B, t|x_A, 0)}{\pi_B(x_A)} \propto \lim_{\theta\to 0} q(x_B, t|x_A+\theta, 0). \tag{9}$$

In what follows, we take $x_A = -1$ and $x_B = 1$.

2.2. Coefficient of variation

We use the coefficient of variation C_V to analyze the width of the TPTD $\rho(t)$, i.e.

$$C_V = \frac{1}{\langle t_{\mathrm{TP}}\rangle}\left(\langle t_{\mathrm{TP}}^2\rangle - \langle t_{\mathrm{TP}}\rangle^2\right)^{1/2}, \tag{10}$$

where $\langle t_{\mathrm{TP}}\rangle$ and $\langle t_{\mathrm{TP}}^2\rangle$ are the mean and the second moment of the TPT from $x_A(x_B)$ to $x_B(x_A)$, given the absorbing boundary conditions at x_A and x_B. These moments are generally defined as

$$\langle t_{\mathrm{TP}}^n\rangle = \int_0^\infty t^n \rho(t)\,\mathrm{d}t, \tag{11}$$

for integer n. We note that broad distributions have a large C_V.

3. Algorithm for calculating the transition path times

Equation (4) is simulated by first transforming the generalized Langevin equation into a system of ordinary differential equations containing Gaussian white noise, and then using the Runge Kutta algorithm [81]. For our simulations, we use the FFS to obtain the TPTD $\rho(t)$, then C_V is derived from equations (10) and (11). The random force $\epsilon(t)$ can be produced from two Ornstein–Uhlenbeck noises driven by the same white Gaussian noise $\eta(t)$ of unit strength,

$$\epsilon(t) = \epsilon_1(t) + \epsilon_2(t), \tag{12a}$$

$$\dot{\epsilon}_1(t) = -\frac{1}{\tau_1}\epsilon_1(t) + \frac{1}{\tau_1}\sqrt{2k_BT\alpha_1}\eta(t), \tag{12b}$$

$$\dot{\epsilon}_2(t) = -\frac{1}{\tau_2}\epsilon_2(t) + \frac{1}{\tau_2}\sqrt{2k_BT\alpha_2}\eta(t). \tag{12c}$$

Then, we can convert equation (4) into a system of two Markovian Langevin equation by introducing the variables

$$y_1(t) = \alpha_1 \int_0^t \frac{1}{\tau_1} \exp\left(-\frac{t-s}{\tau_1}\right) \dot{x}(s)\,\mathrm{d}s - \epsilon_1(t), \tag{13a}$$

$$y_2(t) = \alpha_2 \int_0^t \frac{1}{\tau_2} \exp\left(-\frac{t-s}{\tau_2}\right) \dot{x}(s)\,\mathrm{d}s - \epsilon_2(t). \tag{13b}$$

Substituting equations (12) and (13) into equation (4) we obtain

$$\dot{x}(t) = -\frac{1}{2\alpha_0}\left(y_1(t) + y_2(t) + f(x)\right), \tag{14a}$$

$$\dot{y}_1(t) = -\frac{\alpha_1 + 2\alpha_0}{2\alpha_0\tau_1} y_1(t) - \frac{\alpha_1}{2\alpha_0\tau_1} y_2(t) - \frac{\alpha_1}{2\alpha_0\tau_1} f(x) - \frac{1}{\tau_1}\sqrt{2k_BT\alpha_1}\,\eta(t), \tag{14b}$$

$$\dot{y}_2(t) = -\frac{\alpha_2 + 2\alpha_0}{2\alpha_0\tau_2} y_2(t) - \frac{\alpha_2}{2\alpha_0\tau_2} y_1(t) - \frac{\alpha_2}{2\alpha_0\tau_2} f(x) - \frac{1}{\tau_2}\sqrt{2k_BT\alpha_2}\,\eta(t). \tag{14c}$$

Based on this Markovian formulation, simulations using the Runge–Kutta method and the FFS scheme can be employed to obtain the transition path properties of equation (4).

4. Approximate theoretical solution of the transition path time distribution and the mean transition path time

4.1. Transition path time distribution

For the two different potentials, we now discuss the associated transition path properties. For the inverted parabolic potential $U(x) = -kx^2/2$, the time-dependent diffusion coefficient is given by [77]

$$D(t) = \frac{1}{\beta k}\frac{\mathrm{d}}{\mathrm{d}t}\log\left(\chi(t)\right), \tag{15}$$

where $\chi(t)$ has the form

$$\chi(t) = \mathscr{L}^{-1}\left\{\frac{\hat{\xi}(s)}{s\hat{\xi}(s) - k}\right\}. \tag{16}$$

Here $\mathscr{L}^{-1}\{\cdot\}$ denotes the inverse Laplace transform, and according to equation (2), we have

$$\hat{\xi}(s) = \alpha_0 + \frac{\alpha_1}{1+\tau_1 s} + \frac{\alpha_2}{1+\tau_2 s}, \tag{17}$$

$\hat{\xi}(s)$ is the Laplace transform of the friction kernel $\xi(t)$, $\hat{\xi}(s) = \mathscr{L}\{\xi(t)\} = \int_0^\infty \xi(t)\exp(-st)\mathrm{d}t$.

In the opposite case of the parabolic potential $U(x) = kx^2/2$, the time-dependent diffusion coefficient reads

$$D(t) = -\frac{1}{\beta k}\frac{\mathrm{d}}{\mathrm{d}t}\log\left(\chi(t)\right), \tag{18}$$

and $\chi(t)$ is given by

$$\chi(t) = \mathscr{L}^{-1}\left\{\frac{\hat{\xi}(s)}{s\hat{\xi}(s)+k}\right\}. \tag{19}$$

We now define $F(s) = \hat{\xi}(s)/[s\hat{\xi}(s)-k]$, and then combine with equation (17), we obtain

$$F(s) = \frac{\alpha_0\tau_1\tau_2 s^2 + [\alpha_0(\tau_1+\tau_2)+\alpha_2\tau_1-\alpha_1\tau_2]s + \alpha_0+\alpha_2-\alpha_1}{\alpha_0\tau_1\tau_2 s^3 + [\alpha_0(\tau_1+\tau_2)+\alpha_2\tau_1-\alpha_1\tau_2-k\tau_1\tau_2]s^2 + [\alpha_0+\alpha_2-\alpha_1-k(\tau_1+\tau_2)]s - k}. \tag{20}$$

Given the chosen system parameters, via factorizaion equation (20) can be brought to the form

$$F(s) = \frac{K_1}{s-P_1} + \frac{K_2}{s-P_2} + \frac{K_3}{s-P_3}, \tag{21}$$

where the P_i $(i=1,2,3)$ are three solutions of the equation $s\hat{\xi}(s)-k=0$, and $K_i = (s-P_i)F(s)|_{s=P_i}$, $(i=1,2,3)$. The same approach can be used for equation (19), except that the values of K_i and P_i are different in this case. For the system parameters we chose, P_i are all real roots. Hence, we can write the general form

$$\chi(t) = K_1 e^{P_1 t} + K_2 e^{P_2 t} + K_3 e^{P_3 t}, \tag{22}$$

for both parabolic and inverse-parabolic potentials.

When the potential barrier is high, it is highly unlikely that a particle leaving the region (x_A, x_B) will return into this interval if we replace the absorbing boundary conditions with natural boundary conditions, i.e. $\lim_{|x|\to\infty} P(x,t|x_0,0) = 0$. Therefore, the solution of equation (5) obtained for natural boundary conditions is expected to be a good approximation of our case here with two absorbing boundaries. For natural boundary conditions the solution of equation (5) with $U(x) = -kx^2/2$ has the Gaussian form [77]

$$P(x,t|x_0,0) = \left(\frac{2\pi}{\beta k}\left[\xi^2(t)-1\right]\right)^{-1/2} \exp\left(-\frac{\beta k[x-\xi(t)x_0]}{2[\xi^2(t)-1]}\right). \tag{23}$$

Conversely, for $U(x) = kx^2/2$, we have

$$P(x,t|x_0,0) = \left(\frac{2\pi}{\beta k}\left[1-\xi^2(t)\right]\right)^{-1/2} \exp\left(-\frac{\beta k[x-\xi(t)x_0]}{2[1-\xi^2(t)]}\right). \tag{24}$$

Combined with equation (8), for the case of $U(x) = -kx^2/2$, we find

$$q(x_B,t|x_A,0) = \sqrt{\frac{\beta k x_B^2}{2\pi}}\frac{\dot{\chi}(t)}{(\chi(t)-1)\sqrt{\chi^2(t)-1}} \exp\left(-\frac{\beta k x_B^2}{2}\left[\frac{\chi(t)+1}{\chi(t)-1}\right]\right). \tag{25}$$

Similarly, for $U(x) = kx^2/2$,

$$q(x_B,t|x_A,0) = -\sqrt{\frac{\beta k x_B^2}{2\pi}}\frac{\dot{\chi}(t)}{(1-\chi(t))\sqrt{1-\chi^2(t)}} \exp\left(-\frac{\beta k x_B^2}{2}\left[\frac{1+\chi(t)}{1-\chi(t)}\right]\right). \tag{26}$$

To gain more insight into the exact behavior of the one-side TPTD, we proceed to analyze the shape of the distribution in the short-time and long-time limits. From equations (9) and (25), at short times ($t \to 0$),

$$-\log(\rho(t)) \sim -\sqrt{\frac{\beta k x_B^2}{2\pi}} - \log(\dot{\chi}(t)) + \log(\chi(t)-1) + \frac{1}{2}\log\left(\chi^2(t)-1\right) + \frac{\beta k x_B^2}{2}\left[1+\frac{2}{\chi(t)-1}\right], \tag{27}$$

and the leading term is

$$-\log(\rho(t)) \sim \frac{\beta k x_B^2}{2}\left[1+\frac{2}{\chi(t)-1}\right] \sim \frac{\beta k x_B^2 t^{-1}}{K_1P_1+K_2P_2+K_3P_3}, \tag{28}$$

for $U(x) = -kx^2/2$. In the opposite case $U(x) = kx^2/2$, the short-time behavior is derived from equation (26),

$$-\log(\rho(t)) \sim -\frac{\beta k x_B^2}{2}\left[\frac{2}{1-\chi(t)}-1\right] \sim -\frac{\beta k x_B^2 t^{-1}}{K_1P_1+K_2P_2+K_3P_3}. \tag{29}$$

For the case $U(x) = -kx^2/2$, we find the long-time ($t \to \infty$) asymptote from equation (9),

$$\log(\rho(t)) \sim \log\left(K_2 e^{P_2 t}\right) - \log\left(K_2P_2 e^{P_2 t}\right) - \frac{1}{2}\log\left(K_2^2P_2 e^{2P_2 t}\right) \sim -P_2 t. \tag{30}$$

However, the long-time behavior of the TPTD for the parabolic potential $U(x) = kx^2/2$ is more involved. For our parameters we find that for $t \in (0, 0.2)$,

$$\log(\rho(t)) \sim \log(-\dot{\chi}(t)) \sim \log\left(-K_1 e^{P_1 t}\right) \sim P_1 t, \tag{31}$$

while for $t \in (0.2, 6)$,

$$\log(\rho(t)) \sim \log(-\dot{\chi}(t)) \sim \log\left(-K_3P_3 e^{P_3 t}\right) \sim P_3 t, \tag{32}$$

and for $t \in (14, +\infty)$,

$$\log(\rho(t)) \sim \log(-\dot{\chi}(t)) \sim \log\left(-K_2P_2 e^{P_2 t}\right) \sim P_2 t. \tag{33}$$

This is very different from the long-time behavior of the TPTD for the inverted parabolic potential case.

4.2. Transition path time

We now proceed to consider the mean TPT. To this end we introduce the absorption function $Q_A(t)$, defined by [16]

$$Q_A(t) = \int_{x_0}^{\infty} P(x, t|x_0, 0)\,\mathrm{d}x. \tag{34}$$

The value of $Q_A(t+\triangle t)-Q_A(t)$ is the fraction of the trajectories that the particles cross x_0 in the interval $[t,t+\triangle t]$, thus the TPTD $\rho(t)$ can be approximated as [16]

$$\rho(t)\approx\mathscr{N}\frac{\mathrm{d}Q_A(t)}{\mathrm{d}t}, \tag{35}$$

with the normalization factor $\mathscr{N}$. From the normalization of the TPTD, we then find

$$\int_0^\infty \rho(t)\,\mathrm{d}t=\mathscr{N}\left[Q_A(\infty)-Q_A(0)\right], \tag{36}$$

and $Q_A(0)=0$. Hence, $\mathscr{N}=\frac{1}{Q_A(\infty)}$, and $Q_A(\infty)=\lim\limits_{t\to\infty}Q_A(t)$.

For the case $U(x)=-\frac{1}{2}kx^2$, combining equations (23) and (34) we obtain

$$Q_A(t)=\frac{1}{2}\left[1-\mathrm{erf}\left(G(t)\right)\right], \tag{37}$$

where $\mathrm{erf}(x)=(2/\sqrt{\pi})\int_0^x\exp(-t^2)dt$ is the error function and

$$G(t)=\sqrt{\beta E}\sqrt{\frac{\chi(t)+1}{\chi(t)-1}}. \tag{38}$$

Here we used the abbreviation $E=kx_B^2/2$. The function $G(t)$ is monotonically decreasing in time t. In this case, $Q_A(\infty)=(1/2)\left[1-\mathrm{erf}(\sqrt{\beta E})\right]$.

Hence, according to equation (35), the TPTD (9) can be rewritten in the form

$$\rho(t)=-\frac{2}{\sqrt{\pi}}\frac{\dot{G}(t)\,e^{-G^2(t)}}{1-\mathrm{erf}\left(\sqrt{\beta E}\right)}. \tag{39}$$

Therefore, the mean TPT assumes the form

$$\langle t_{\mathrm{TP}}\rangle=\int_{\sqrt{\beta E}}^\infty t(G)\,e^{-G^2}\mathrm{d}G\Big/\int_{\sqrt{\beta E}}^\infty e^{-G^2}\mathrm{d}G. \tag{40}$$

We can get the approximate solution for the mean TPT for $\beta E\gg 1$ when the integrals are determined by the large t-limit of $G(t)$. According to equation (38), we then obtain

$$t=\frac{1}{P_2}\log\left(\frac{1}{K_2}\frac{G^2+\beta E}{G^2-\beta E}\right). \tag{41}$$

We then use the integral variable substitution, and define $x=G^2-\beta E$,

$$\begin{aligned}\langle t_{\mathrm{TP}}\rangle=&-\frac{1}{P_2}\int_0^\infty\left[\log(2)+\log(\beta E)+\log\left(1+x/\left[\beta E\right]\right)-\log(K_2)-\log(x)\right]e^{-x}\\&\times\left(1+\frac{x}{\beta E}\right)^{-1/2}\mathrm{d}x\Big/\int_0^\infty\frac{1}{\sqrt{1+\frac{x}{\beta E}}}e^{-x}\mathrm{d}x\\\approx&\frac{1}{P_2}\log\left(\frac{2\beta E e^C}{K_2}\right)+O\left(\frac{1}{\beta E}\right),\end{aligned} \tag{42}$$

O is the Landau symbol and $C = -\int_0^\infty \log(x) e^{-x} \mathrm{d}x \approx 0.577\,215$ is the Euler–Mascheroni constant.

For the case $U(x) = \frac{1}{2}kx^2$, according to equation (26) we define

$$G(t) = \sqrt{\beta E}\sqrt{\frac{1+\chi(t)}{1-\chi(t)}}, \tag{43}$$

and we obtain $t = (1/P_2)\log\left(\frac{1}{K_2}\frac{G^2-\beta E}{G^2+\beta E}\right)$ from equation (43). In the large t-limit of $G(t)$, we can also determine the approximate solution of the mean TPT for $\beta E \gg 1$,

$$\begin{aligned}\langle t_{\mathrm{TP}}\rangle &= \int_{\sqrt{\beta E}}^{\infty} t(G)\, e^{-G^2}\mathrm{d}G \Big/ \int_{\sqrt{\beta E}}^{\infty} e^{-G^2}\mathrm{d}G \\ &= (1/P_2)\int_0^{\infty} \left[\log(x) - \log(2) - \log(\beta E) - \log\left(1 + x/[\beta E]\right) - \log(K_2)\right] e^{-x} \\ &\quad \times \left(\sqrt{1+\frac{x}{\beta E}}\right)^{-1/2} \mathrm{d}x \Big/ \int_0^{\infty} \frac{1}{\sqrt{1+\frac{x}{\beta E}}} e^{-x}\mathrm{d}x \\ &\approx -\frac{1}{P_2}\log\left(2K_2\beta E e^{C}\right) + O\left(\frac{1}{\beta E}\right).\end{aligned} \tag{44}$$

This completes our approximate derivation of the mean TPT for the two external potentials in the limit $\beta E \gg 1$.

5. Results

We now present a detailed study of the transition path properties for the two generic examples of the external potential, the parabolic and the inverted parabolic potentials. In particular, we compare our approximate analytical results with stochastic simulations using the FFS simulation method, reporting good agreement. For increasing force constant k the agreement improves progressively. In the discussion of the coefficient of variation we find that it can exceed unity in the parabolic potential case.

5.1. Transition path time distribution

The effect of the system parameters on the TPTD of the (inverted) parabolic potentials is shown in figures 2–4. Panels (a) and (b) in figure 2 show the variation of the TPTD with the force constant k. It is distinct that k strongly affects the TPTD. As the strength of the potential increases, the peak value of the TPTD grows, while the TPT corresponding to the maximum is shifting to lower values. Thus the height of the potential barrier accelerates the onset of the particle escape behaviour. The shape of the TPTD narrows as the potential barrier increases. We performed simulations of the TPTD using the FFS algorithm. As seen from the figures, the agreement between our approximative theory and the FFS simulations is excellent for the two sample potentials. Particularly, as expected we see that the deviations between theoretical and numerical results diminish as k decreases.

Panels (c) and (d) of figure 2 display the short-time and long-time behavior of the TPTD for a range of k values of the parabolic potential, while panels (e) and (f) show the results for the inverted parabolic potential. Note the negative logarithm in panel (c) versus inverse time

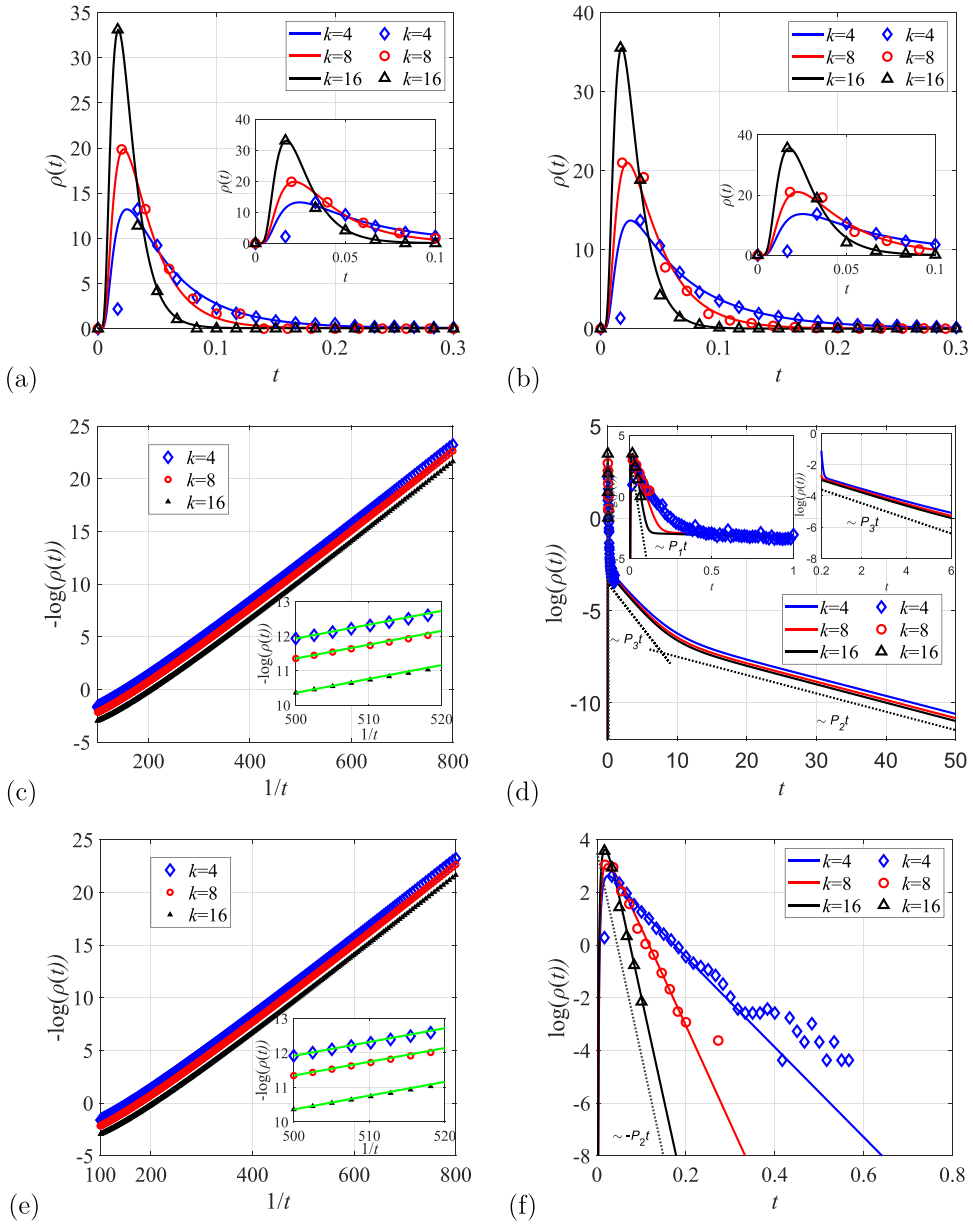

Figure 2. (a) TPTD for parabolic potential $U(x) = kx^2/2$ with $k = 4$, $k = 8$, and $k = 16$. The lines are theoretical results from equations (9) and (26). (b) TPTD for inverted parabolic potential $U(x) = -kx^2/2$ for the same k-values, the lines are theoretical results from equations (9) and (25). In (a) and (b), these symbols are also the simulation results. (c) Short-time exponential behaviour in the parabolic potential. The lines are analytic results in equation (29), the symbols represent the results from equation (9). (d) Long-time exponential behaviour in the parabolic potential, the lines are analytic results in equations (9) and (31)–(33), the symbols represent the FFS results. (e) Short-time exponential behaviour for the inverted parabolic potential, the lines are analytic results from equation (28), the symbols represent the theoretiacl results from equation (9). (f) Long-time exponential behaviour for the inverted parabolic potential, the lines are analytic results in equation (30), the symbols represent the numerical results. The insets of panels (c) and (e) show the short-time behavior of the TPTD. The inset of panel (d) reveals the long-time behavior of the TPTD of the parabolic potential case.

in panels (c) and (e). In panel (c) it is evident that the growth of the force constant k leads to an increase in the TPTD, in analogy to the behavior for the inverted parabolic potential in panel (e): an increase in the height of the potential barrier leads to an increase of the amplitudes in the TPTD at short times. Note that in panels (c) and (d) symbols denote the results of equation (9) and green lines in the insets are the approximate short-time results of equations (28) and (29). For the case $U(x) = kx^2/2$ the long-time asymptotic behavior of the TPTD is shown in panel (d), corresponding to equations (31)–(33), depicted by black dashed lines, while the black solid lines represent the approximate theoretical results of equation (9). Note that for clarity we only show the comparison over all times for the case $k = 16$. Similarly, panel (f) shows the results for the inverted parabolic potential, in comparison with equation (30) (black dashed line). We note again that the agreement is improving for increasing potential strength.

In figure 3 we display the variation of the TPTD with the system parameters for the parabolic potential case. Panels (a)–(d) show the TPTD for various values of the parameters α_0, β, α_1, and α_2. As shown in panel (a) the height of the TPTD peak decreases as α_0 increases. The same influence of β, α_1, and α_2 on the height of the TPTD can be seen in panels 3(b)–(d). From panels (c) and (d) we conclude that the effect of α_2 on the TPTD is stronger as that of α_1. While the effect is not too strong, we see that increasing values of α_1 and α_2 lower the time for the most likely TPT and thus accelerate the transition dynamics. As presented in panels (e) and (f), the effect of increasing τ_1 and τ_2 on the TPTD peak leads to a decrease of the TPTD peak while the tails become heavier. From all panels we conclude that the effect of the parameters α_0, β, τ_1, and τ_2 is a deceleration. We note that, again, the agreement between theoretical results and simulations is very good.

Figure 4 is the inverted parabolic potential case. We similarly consider the effect of the system parameters on the TPTD. The trend of the effects is consistent with the results presented in figure 3. In particular, we chose the same parameter values and it can be noticed that for the parabolic potential function case, the influence of α_1, α_2, τ_1, and τ_2 on the TPTD is stronger than for the inverted parabolic potential case.

5.2. *Mean transition path time and coefficient of variation*

We now turn to the behavior of mean TPT. In figure 5, we show simulations results for the mean TPT obtained from the FFS scheme as a function of βE for the two potential scenarios and compare them with the theoretical results from equations (11), (42) and (44). We see that as βE increases, the approximate theoretical results (42) and (44) show an improving match to equation (11). Moreover, the comparison with the simulations shows that our approximate theoretical result is reproducing the dynamics of the system adequately.

We now turn to the influence of the two decay times τ_1 and τ_2 on the mean TPT, while we choose $\alpha_1 = \alpha_2$. Based on equation (11), we consider the asymmetric case when $\tau_1 \neq \tau_2$ in figure 6. Panels (a) and (b) show how the mean TPT for $U(x) = kx^2/2$ varies with τ_1 when $\tau_2 \ll \tau_1$. Panel (a) shows $\langle t_{\mathrm{TP}} \rangle / \tau_D$ as a function of τ_1/τ_D for fixed $\tau_2/\tau_D = 10$ and some varying values of τ_m/τ_D. For $\tau_1 \gg \tau_2$ and $\tau_1 > \tau_D$, it can be seen that the mean TPT becomes asymptotically independent of τ_1. We also observe a similar trend in panel (b), where we fixed $\tau_m/\tau_D = 0.01$: here the mean TPT also becomes independent of τ_1 when $\tau_1 \gg \tau_2$ and $\tau_1 > \tau_D$. As we chose $\alpha_1 = \alpha_2$, if we assume that $\tau_2 > \tau_D$ and $\tau_2 \gg \tau_1$ and then consider the variation of $\langle t_{\mathrm{TP}} \rangle / \tau_D$ with τ_2/τ_D, we could obtain consistent results with panels (a) and (b), with the mean

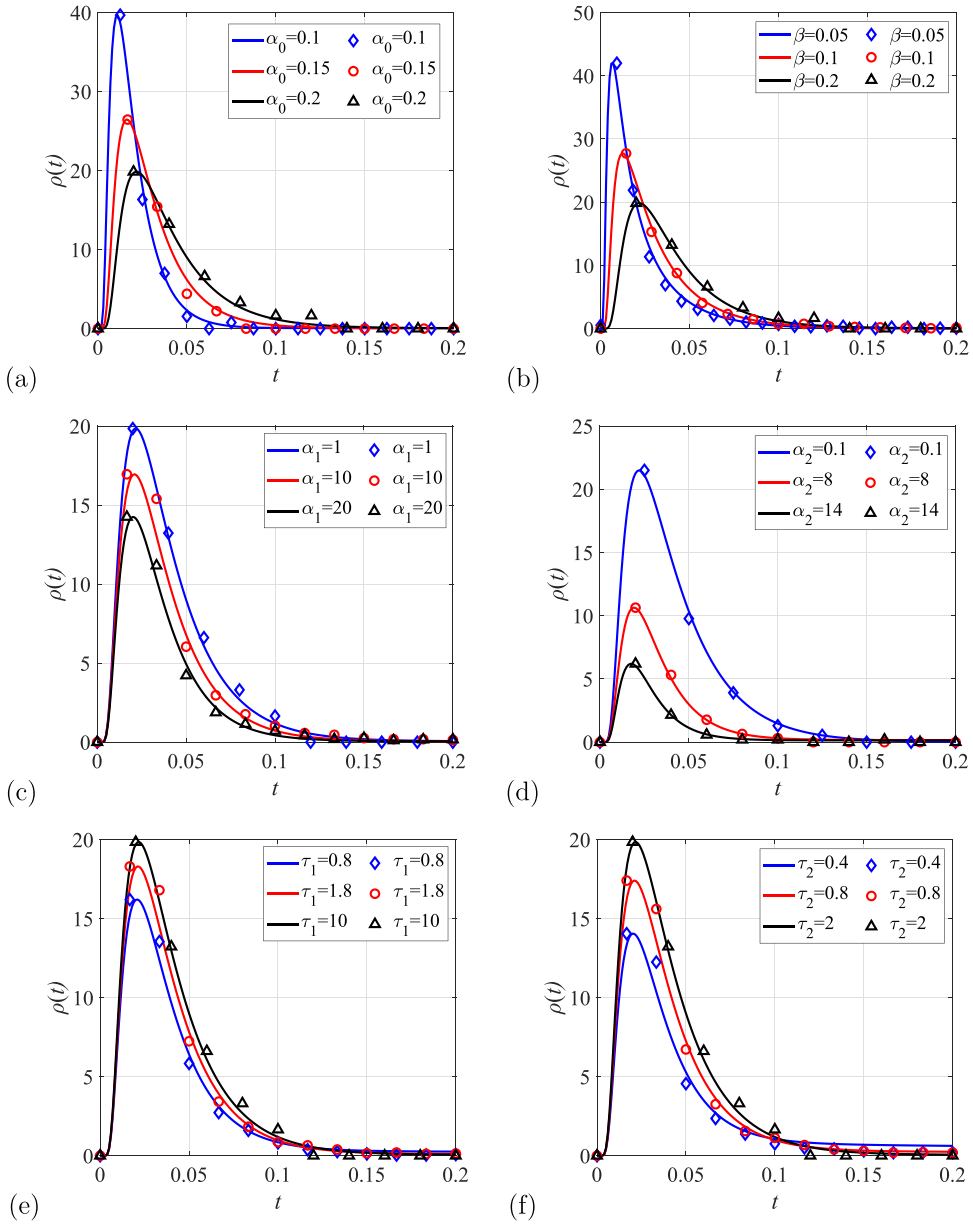

Figure 3. TPTD for $U(x) = kx^2/2$ with $k = 8$ for different system parameters. (a) Varying α_0 for $\beta = 0.2$: $\alpha_1 = 1$, $\alpha_2 = 1$, and $\tau_1 = 10$ and $\tau_2 = 2$. (b) Varying β for $\alpha_0 = 0.2$, $\alpha_1 = 1$, $\alpha_2 = 1$, $\tau_1 = 10$, and $\tau_2 = 2$. (c) Varying α_1 for $\alpha_0 = 0.2$, $\beta = 0.2$, $\alpha_2 = 1$, $\tau_1 = 10$, and $\tau_2 = 2$. (d) Varying α_2 for $\alpha_0 = 0.2$, $\beta = 0.2$, $\alpha_1 = 1$, $\tau_1 = 10$, and $\tau_2 = 2$. (e) Varying τ_1 for $\alpha_0 = 0.2$, $\beta = 0.2$, $\alpha_1 = 1$, $\alpha_2 = 1$, and $\tau_2 = 2$. (f) Varying τ_2 for $\alpha_0 = 0.2$, $\beta = 0.2$, $\alpha_1 = 1$, $\alpha_2 = 1$, and $\tau_1 = 10$. In the figures, the lines are analytic results, the symbols represent the numerical results.

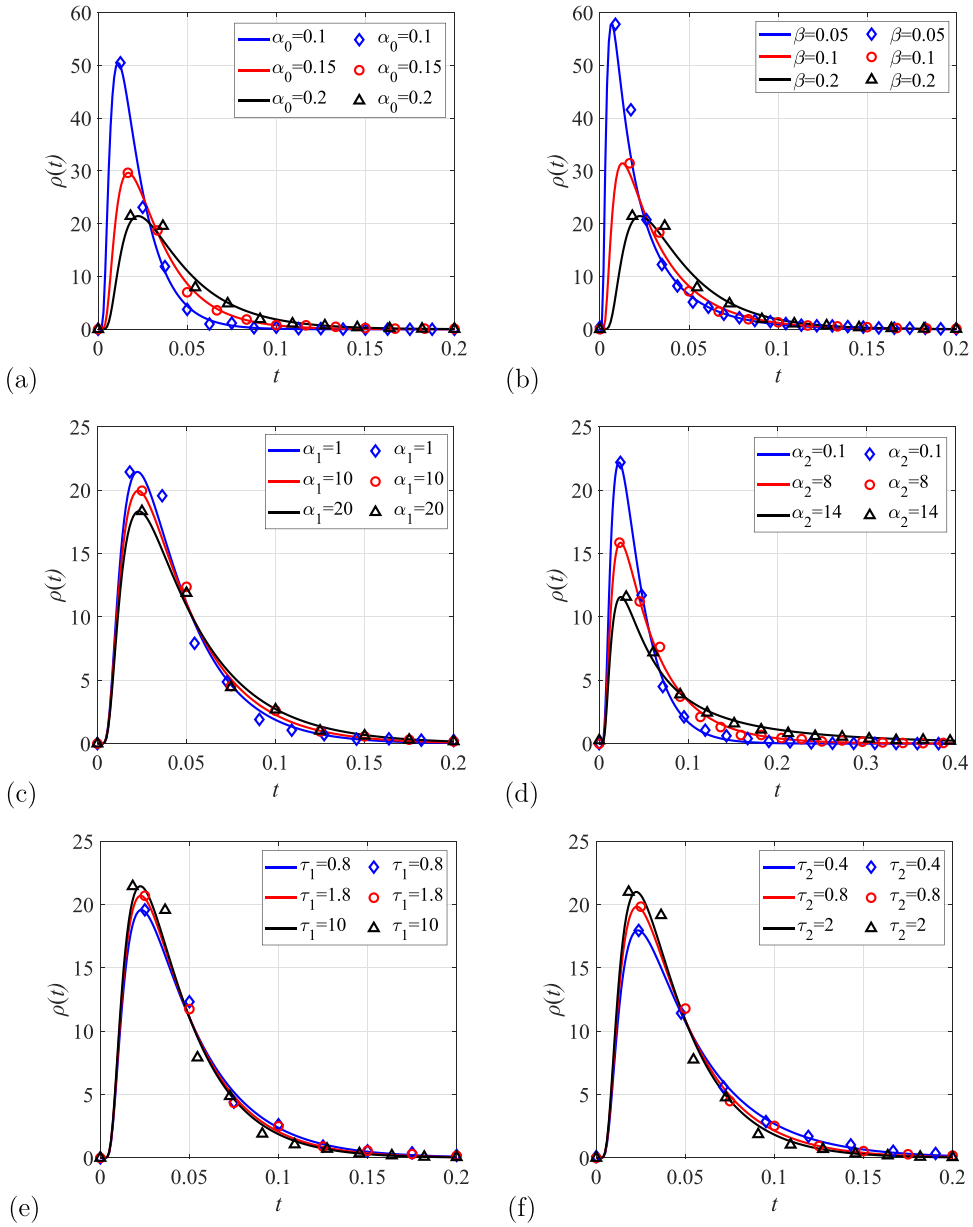

Figure 4. TPTD for $U(x) = -kx^2/2$ with $k = 8$ for different system parameters. (a) Varying α_0 for $\beta = 0.2$, $\alpha_1 = 1$, $\alpha_2 = 1$, $\tau_1 = 10$, and $\tau_2 = 2$. (b) Varying β for $\alpha_0 = 0.2$, $\alpha_1 = 1$, $\alpha_2 = 1$, $\tau_1 = 10$, and $\tau_2 = 2$. (c) Varying α_1 for $\alpha_0 = 0.2$, $\beta = 0.2$, $\alpha_2 = 1$, $\tau_1 = 10$, and $\tau_2 = 2$. (d) Varying α_2 for $\alpha_0 = 0.2$, $\beta = 0.2$, $\alpha_1 = 1$, $\tau_1 = 10$, and $\tau_2 = 2$. (e) Varying τ_1 for $\alpha_0 = 0.2$, $\beta = 0.2$, $\alpha_1 = 1$, $\alpha_2 = 1$, and $\tau_2 = 2$. (f) Varying τ_2 for $\alpha_0 = 0.2$, $\beta = 0.2$, $\alpha_1 = 1$, $\alpha_2 = 1$, and $\tau_1 = 10$. The lines are analytic results, the symbols represent the numerical results.

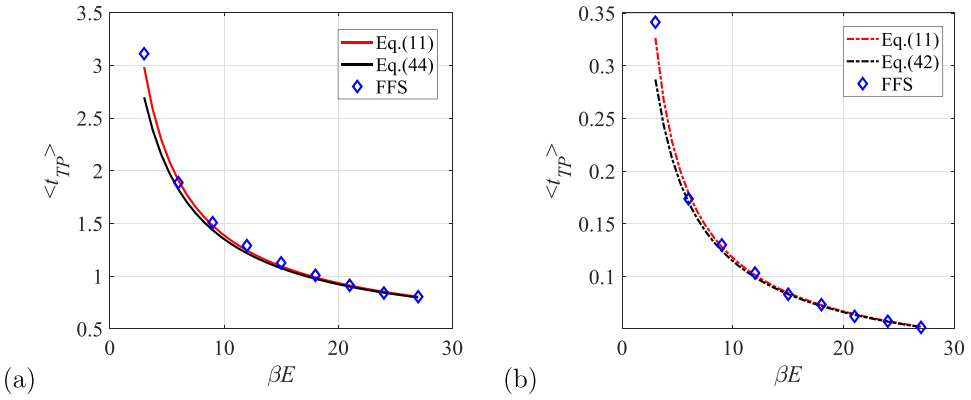

Figure 5. (a) Mean TPT for $U(x) = kx^2/2$ with $\alpha_0 = 0.2$, $\alpha_1 = \alpha_2 = 1$, $\tau_1 = 0.1$, $\tau_2 = 0.05$, $\beta = 3$, and $k = 2 : 0.5 : 18$. (b) Mean TPT for $U(x) = -kx^2/2$ with $\alpha_0 = 0.2$, $\alpha_1 = \alpha_2 = 1$, $\tau_1 = 10$, $\tau_2 = 2$, $\beta = 3$, and $k = 2 : 0.5 : 18$.

TPT becoming progressively independent of τ_2. The black dotted horizontal lines at higher τ_1/τ_D values in figure 6 demonstrate the dependence of the mean TPT on τ_1. Panels (c) and (d) display the case of $U(x) = -kx^2/2$. If we define $\tau_1 \gg \tau_2$ and take $\tau_1 > \tau_D$, the mean TPT becomes almost independent of τ_1. Therefore, we conclude that the mean TPT is dominated by the smaller of the two time scales τ_1 and τ_2 when $\tau_1 > \tau_D$ and $\tau_2 > \tau_D$.

We now continue to consider the coefficient of variation for the TPTD. In figure 7 we show various examples for the (inverted) parabolic potential along with the corresponding TPTD. The width of the TPTD becomes narrower as the potential barrier increases for $U(x) = -kx^2/2$. However, for $U(x) = kx^2/2$ case, we see exactly the opposite trend. The tail of the TPTD for the parabolic potential function is heavier than for the inverted parabolic potentiel.

For the parabolic potential case, we see from figure 8 how the coefficient of variation of the TPTD depends on the system parameters α_0, β, α_1, α_2, τ_1, and τ_2. We see that in all considered cases the coefficient of variation by far exceeds unity. Moreover, it is a monotonic function of the potential stiffness k. Panel (a) shows, for our chosen parameters, that C_V is increasing with increasing k, and it also becomes smaller for increasing α_0. Panels (b)–(d) revearl the same trend for different β, α_1, and α_2 values. Panel (b) portrays C_V as a function of k for fixed values of $\alpha_0 = 0.2$, $\alpha_1 = \alpha_2 = 1$, $\tau_1 = 10$, and $\tau_2 = 2$. With an increase of k, C_V also increases. The effect of α_1 and α_2 on C_V is studied in panels (c) and (d), showing that C_V increases with a growing α_0, β, α_1, and α_2. This behavior is quite different from the effect of τ_1 and τ_2 on C_V.

The variation of C_V with the system parameters is further considered in figure 9 for the $U(x) = -kx^2/2$ case. From panel (a) it can be seen that C_V gets larger as α_0 increases. This is consistent with the effect of α_1 and α_2 on C_V shown in panels (c) and (d). Panels (b), (e) and (f) show that C_V is decreasing as β, τ_1 and τ_2 increase. Specifically, C_V is decreasing with increasing k. For the parameters chosen here, figure 9 demonstrates that C_V can also be less than unity.

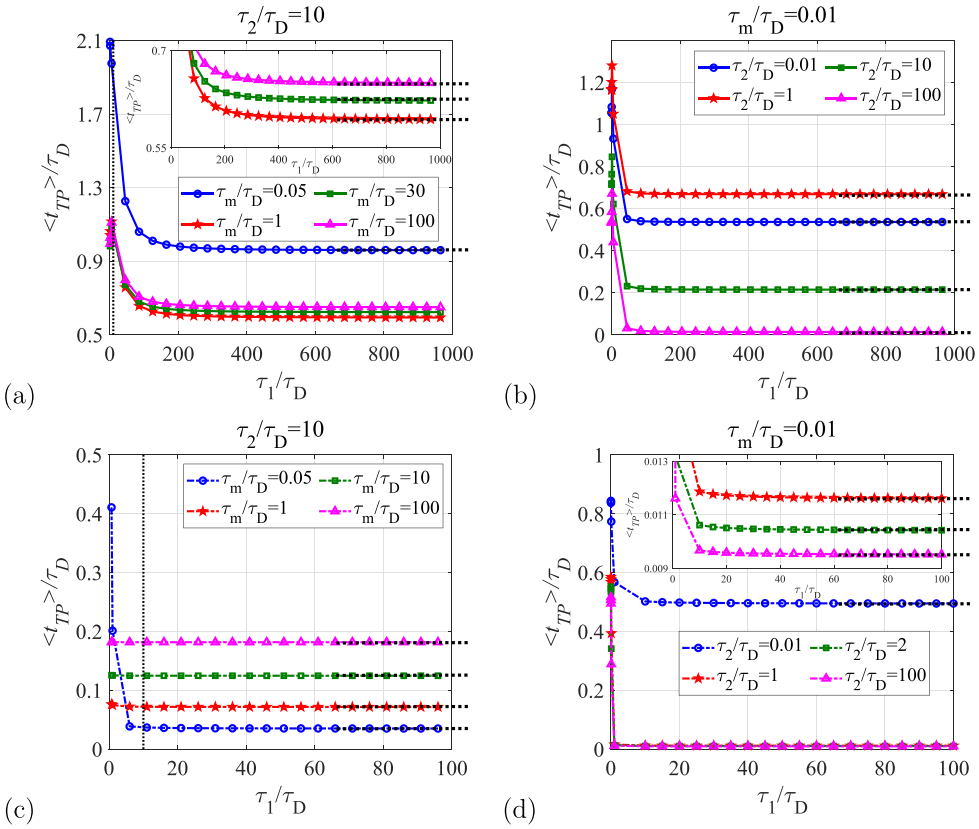

Figure 6. (a) Mean TPT for $U(x) = kx^2/2$ as function of τ_1/τ_D with fixed $\tau_2/\tau_D = 10$, $\alpha_0 = 0.2$, and $\tau_2 = 10$. (b) Mean TPT as function of τ_1/τ_D with fixed $\tau_m/\tau_D = 0.01$ for $U(x) = kx^2/2$, $\alpha_0 = 0.2$, $\beta = 0.2$, and $k = 8$. (a) and (b) are the theoretical results from equations (9), (11) and (26). (c) Mean TPT for $U(x) = -kx^2/2$, as function of τ_1/τ_D with fixed $\tau_2/\tau_D = 10$, $\alpha_0 = 0.2$, and $\tau_2 = 10$. (d) Mean TPT as function of τ_1/τ_D with fixed $\tau_m/\tau_D = 0.01$ for $U(x) = -kx^2/2$, $\alpha_0 = 0.2$, $\beta = 0.2$, and $k = 8$. (c) and (d) are the theoretical results from equations (9), (11) and (25). The vertical dashed line indicates the value of $\tau_1 = \tau_2$ in (a) and (c).

Finally, we also try to generalize our approximate theoretical results to the case of bi-stable potential functions. We consider the mean TPT of the bi-stable potential function for some special regions. As shown in figures 10(a)–(d), we compare the case of overlap between the bi-stable potential function and the inverted parabolic potential function in the transition region $(-1, 1)$. We find that the overlap improves as the height of the potential increases. This being the case, can the theoretical results of mean TPT of the inverted parabolic in the region $(-1, 1)$ be used as an approximation for this bi-stable potential function case? Thus, we compared the theoretical results of equations (11) and (42) for the inverted parabolic potential function with

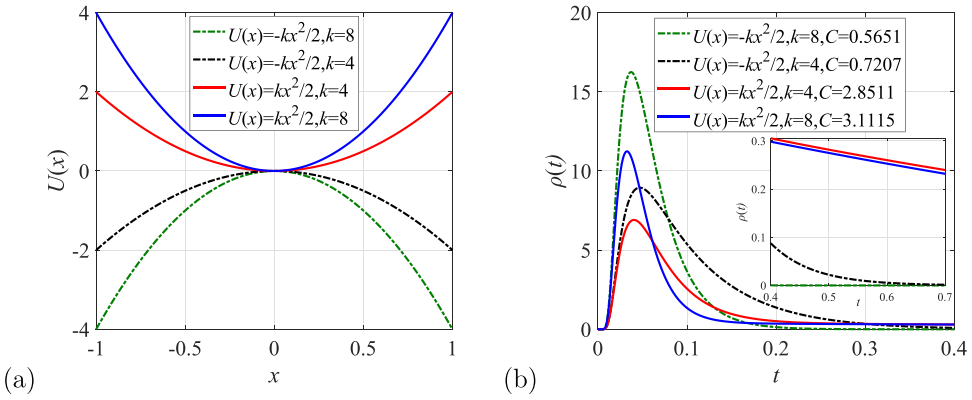

Figure 7. (a) Parabolic potential barrier and potential well for different values of the force constant k. (b) TPTD for the potentials $U(x)$ with the two characteristic shapes from (a) for the parameter values $\alpha_0 = 0.2$, $\tau_1 = 10$, $\tau_2 = 0.8$, $\alpha_1 = 1$, $\alpha_2 = 1$, and $\beta = 0.4$.

the numerical results for the bistable potential function. As shown in figures 10(e) and (f), the fit improves when the height of the potential increases. Therefore, it can be concluded that our theoretical results on the properties of the transition path of this region are acceptable as an approximation to the bistable potential function case.

6. Conclusions

We studied the transition path properties of a one-dimensional non-Markovian stochastic model. In particular, we developed an approximate analytical approach when the memory kernel has a local and two different exponential contributions, to the transition path dynamics for the limit of suffiently high potential barriers. From our discussion of the results and comparison with simulations these approximations are validated. Specifically, we discussed in detail the results for the TPTD and mean TPT for the cases of a parabolic and an inverted parabolic potential. For the parabolic case, the TPTD shows a long tail, becomes more significant as the height of the potential decreases. Concurrently, the mean TPT is independent of the larger of the characteristic time scales τ_1 and τ_2 when the two memory times τ_1 and τ_2 are larger than the intrinsic diffusion time. Furthermore, by controlling the system parameters, we find that for the parabolic potential function, the coefficient of variation of the TPTD exceeds unity, a phenomenon that we ascribe to the inherent multidimensional nature of the dynamics of the system. It is worth mentioning that our theoretical results can also be used as an approximation to the properties of the transiiton path in the case of bi-stable potential functions. As we know, when the potential barrier is relatively high, the bi-stable potential function coincides exactly with the inverted parabolic potential function in certain transition path regions. Therefore, the theoretical results of the transition path properties for the inverted parabolic case can be used as an approximation for the bistable potential function case.

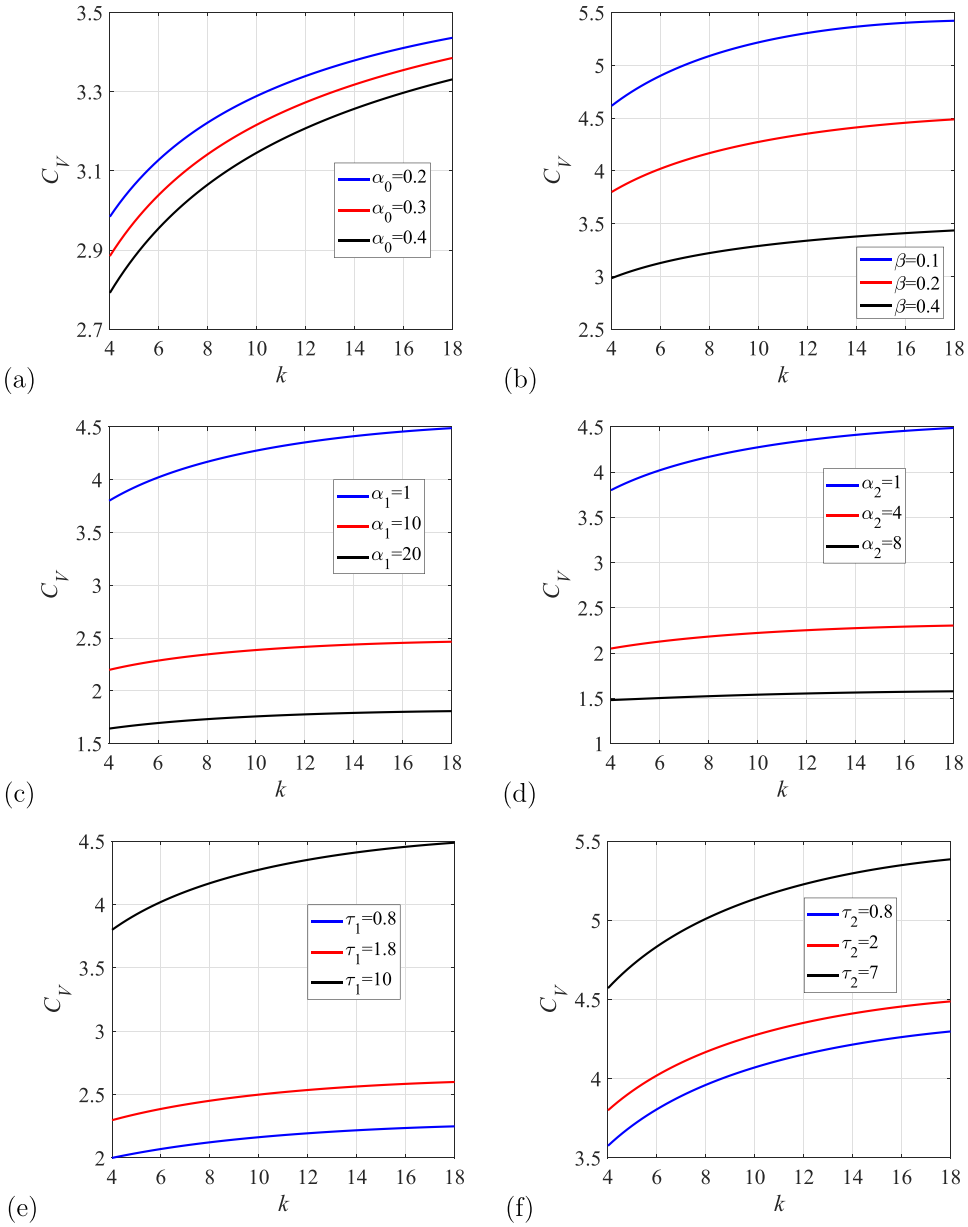

Figure 8. Coefficient of variation of the TPTD for $U(x) = kx^2/2$ with respect to the potential stiffness k. (a) Varying α_0 for $\beta = 0.4$, $\alpha_1 = 1$, $\alpha_2 = 1$, $\tau_1 = 10$, and $\tau_2 = 2$. (b) Varying β for $\alpha_0 = 0.2$, $\alpha_1 = 1$, $\alpha_2 = 1$, $\tau_1 = 10$, and $\tau_2 = 2$. (c) Varying α_1 for $\alpha_0 = 0.2$, $\beta = 0.2$, $\alpha_2 = 1$, $\tau_1 = 10$, and $\tau_2 = 2$. (d) Varying α_2 for $\alpha_0 = 0.2$, $\beta = 0.2$, $\alpha_1 = 1$, $\tau_1 = 10$, and $\tau_2 = 2$. (e) Varying τ_1 for $\alpha_0 = 0.2$, $\beta = 0.2$, $\alpha_1 = 1$, $\alpha_2 = 1$, and $\tau_2 = 2$. (f) Varying τ_2 for $\alpha_0 = 0.2$, $\beta = 0.2$, $\alpha_1 = 1$, $\alpha_2 = 1$, and $\tau_1 = 10$. The lines are analytic results from equations (9)–(11) and (26).

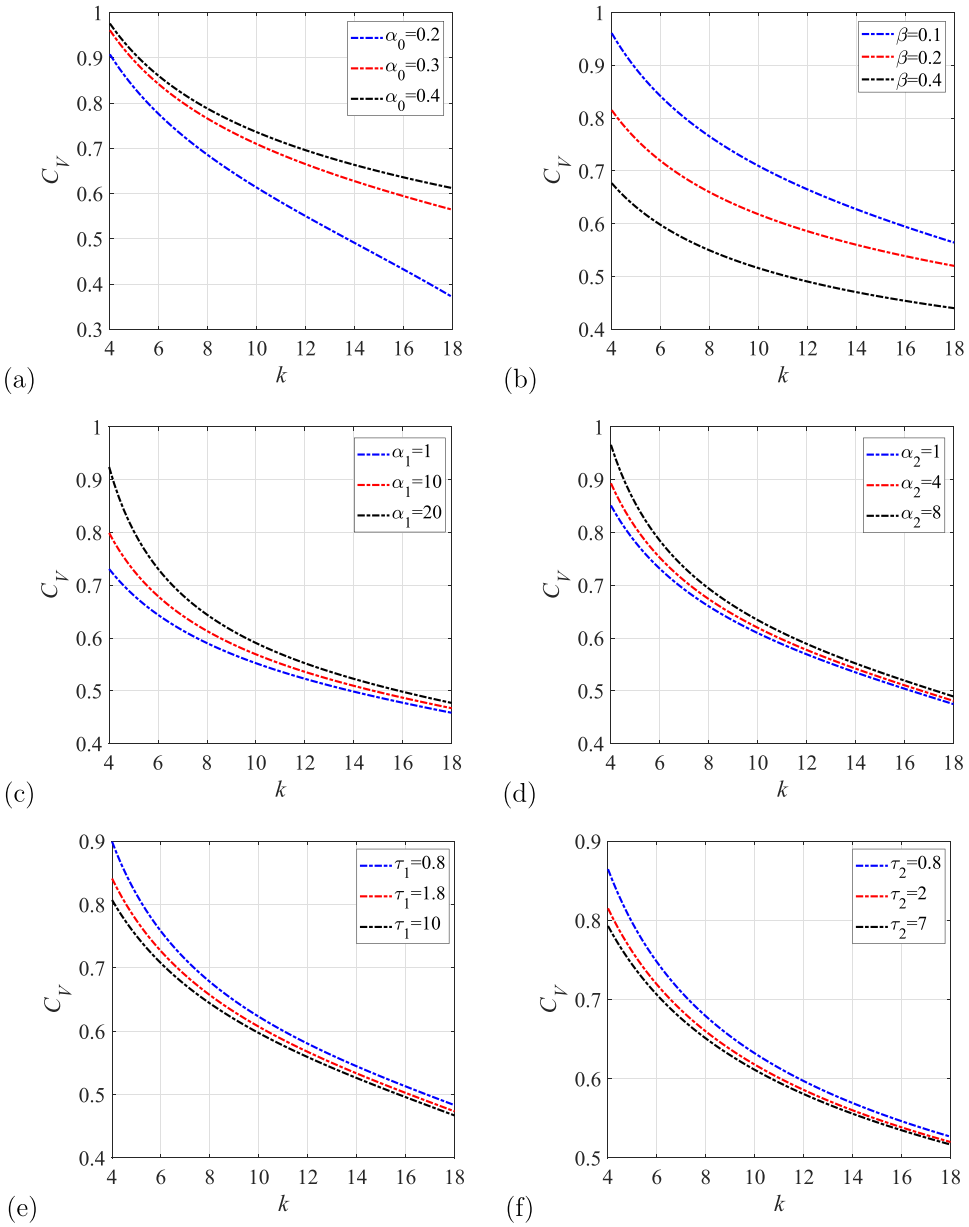

Figure 9. Coefficient of variation of the TPTD for $U(x) = -kx^2/2$ as function of the potential stiffness k. (a) Varying α_0 for $\beta = 0.1$, $\alpha_1 = 1$, $\alpha_2 = 1$, $\tau_1 = 10$, and $\tau_2 = 2$. (b) Varying β for $\alpha_0 = 0.3$, $\alpha_1 = 1$, $\alpha_2 = 1$, $\tau_1 = 10$, and $\tau_2 = 2$. (c) Variung α_1 for $\alpha_0 = 0.2$, $\beta = 0.3$, $\alpha_2 = 1$, $\tau_1 = 10$, and $\tau_2 = 2$. (d) Varying α_2 for $\alpha_0 = 0.2$, $\beta = 0.2$, $\alpha_1 = 1$, $\tau_1 = 10$, and $\tau_2 = 7$. (e) Varying τ_1 for $\alpha_0 = 0.2$, $\beta = 0.2$, $\alpha_1 = 1$, $\alpha_2 = 1$, and $\tau_2 = 2$. (f) Varying τ_2 for $\alpha_0 = 0.3$, $\beta = 0.2$, $\alpha_1 = 1$, $\alpha_2 = 1$, and $\tau_1 = 10$. The lines are analytic results from equations (9)–(11) and (25).

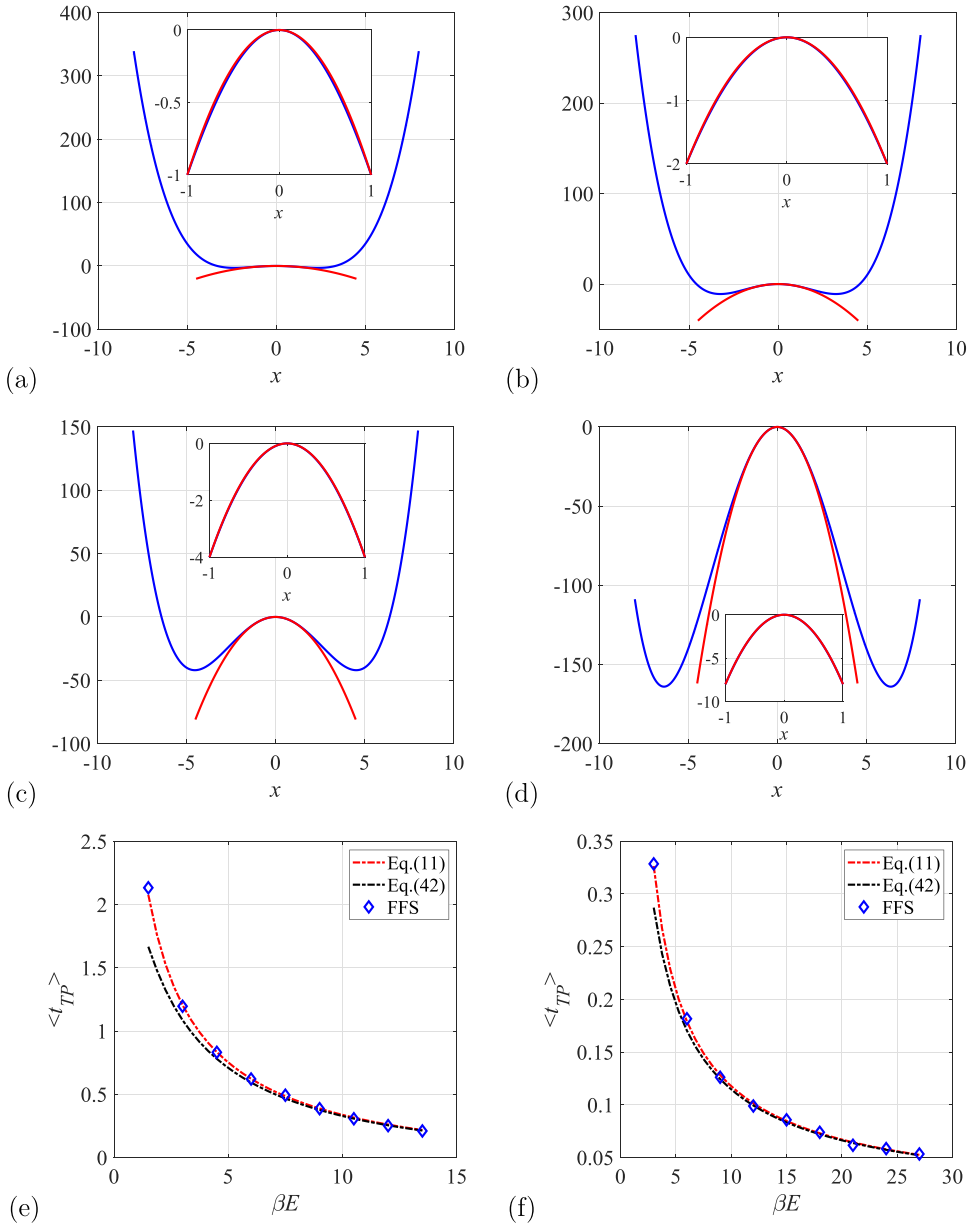

Figure 10. Barrier potential consisting of an inverted parabolic potential $U_1(x) = -kx^2/2$ and bi-stable potential function $U_2(x) = ax^4 - bx^2$. (a) $a = 0.1, b = 1.1, k = 2$; (b) $a = 0.1, b = 2.1, k = 4$; (c) $a = 0.1, b = 4.1, k = 8$; (d) $a = 0.1, b = 8.1, k = 16$. The blue lines in figures (a)–(d) is the bi-stable potential function $U_1(x) = ax^4 - bx^2$, and the red lines are the inverted parabolic potential function $U_2(x) = -kx^2/2$, and the insets of panels (a)–(d) are plots of the two potential functions in the transition region $[-1, 1]$. (e) $\alpha_0 = 0.2$, $\alpha_1 = \alpha_2 = 1$, $\tau_1 = 0.1$, $\tau_2 = 0.05$, $\beta = 1.5$, and $k = 2 : 0.5 : 18, b = 1.1 : 1 : 9.1, a = 0.1$. (f) $\alpha_0 = 0.2, \alpha_1 = \alpha_2 = 1, \tau_1 = 10, \tau_2 = 2, \beta = 3$, and $k = 2 : 0.5 : 18, b = 1.1 : 1 : 9.1, a = 0.1$. The two dashed lines in (e) and (f) are theoretical results for the inverted parabolic potential function from equations (11) and (42), and the symbols are numerical results for the bi-stable potential function case from FFS simulation.

Our results clarify how to approach non-Markovian systems with specified time scales that can then be rewritten as a higher-dimensional system of Markovian dynamic equations. It will be interesting to see how this approach can be generalized to systems with many time scales, as, e.g. used in the Markovian embedding for systems with finite-range inverse power-law memory kernels, or when different shapes of the potentials are used.

Data availability statement

No new data were created or analysed in this study.

Acknowledgments

The authors express their gratitude to the editors and the reviewers for the helpful comments. Y Xu was partially supported by the Key International (Regional) Joint Research Program of the National Science Foundation of China (No. 12120101002), the National Natural Science Foundation of China (No. 12072264). H Li thanks the National Science Foundation of China (12202145). J W Shen thanks the National Science Foundation of China (No. 12272135).

ORCID iDs

Hua Li https://orcid.org/0009-0005-4593-1700
Yong Xu https://orcid.org/0000-0002-8407-4650
Ralf Metzler https://orcid.org/0000-0002-6013-7020
Jianwei Shen https://orcid.org/0000-0003-1289-8674

References

[1] Ma J, Liu Q, Xu Y and Kurths J 2022 Early warning of noise-induced catastrophic high-amplitude oscillations in an airfoil model *Chaos* **32** 033119
[2] Liu Q, Xu Y and Li Y 2023 Complex dynamics of a conceptual airfoil structure with consideration of extreme flight conditions *Nonlinear Dyn.* **111** 14991–5010
[3] Wang Z, Li Y, Xu Y, Kapitaniak T and Kurths J 2022 Coherence-resonance chimeras in coupled HR neurons with alpha-stable Lévy noise *J. Stat. Mech.* 053501
[4] Zhang X, Xu Y, Liu Q and Kurths J 2020 Rate-dependent tipping-delay phenomenon in a thermoacoustic system with colored noise *Sci. China. Technol. Sci.* **63** 2315–27
[5] Xu Y, Li H, Wang H, Yue X and Kurths J 2017 The estimates of the mean first exit time of a bistable system excited by Poisson white noise Trans. ASME, J. Appl. Mech. **84** 091004
[6] Kramers H A 1940 Brownian motion in a field of force and the diffusion model of chemical reactions *Physica* **7** 284–304
[7] Li H, Xu Y, Kurths J and Yue X 2019 Stationary distribution simulation of rare events under colored Gaussinan noise *Eur. Phys. J. B* **92** 1–8
[8] Karagiorgi G, Kasieczka G, Kravitz S, Nachman B and Shih D 2022 Machine learning in the search for new fundamental physics *Nat. Rev. Phys.* **4** 399–412
[9] Hummer G 2004 From transition paths to transition states and rate coefficients *J. Chem. Phys.* **120** 516–23
[10] Zhang B, Jasnow D and Zuckerman D M 2007 Transition-event durations in one-dimensional activated processes *J. Chem. Phys.* **126** 074504
[11] Hoffer N Q, Neupane K, Pyo A G T and Woodside M T 2019 Measuring the average shape of transition paths during the folding of a single biological molecule *Proc. Natl Acad. Sci. USA* **116** 8125–30
[12] Neupane K, Foster D A N, Dee D R, Yu H, Wang F and Woodside M T 2016 Direct observation of transition paths during the folding of proteins and nucleic acids *Biophys. J.* **110** 517a

[13] Chung H S, McHale K, Louis J M and Eaton W A 2012 Single-molecule fluorescence experiments determine protein folding transition path times *Science* **335** 981–4
[14] Goswami K and Metzler R 2023 Effects of active noise on transition-path dynamics *J. Phys. Complex.* **4** 025005
[15] Neupane K, Ritchie D B, Yu H, Foster D A N, Wang F and Woodside M T 2012 Transition path times for nucleic acid folding determined from energy-landscape analysis of single-molecule trajectories *Phys. Rev. Lett.* **109** 068102
[16] Laleman M, Carlon E and Orland H 2017 Transition path time distributions *J. Chem. Phys.* **147** 214103
[17] Thorneywork A L, Gladrow J, Qing Y, Rico-Pasto M, Ritort F, Bayley H, Kolomeisky A B and Keyser U F 2020 Direct detection of molecular intermediates from first-passage times *Sci. Adv.* **6** eaaz4642
[18] Dutta R and Pollak E 2021 What can we learn from transition path time distributions for protein folding and unfolding? *Phys. Chem. Chem. Phys.* **23** 23787–95
[19] Satija R, Berezhkovskii A M and Makarov D E 2020 Broad distributions of transition-path times are fingerprints of multidimensionality of the underlying free energy landscapes *Proc. Natl Acad. Sci. USA* **117** 27116–23
[20] Hartich D and Godec A 2021 Emergent memory and kinetic hysteresis in strongly driven networks *Phys. Rev.* X **11** 041047
[21] Berezhkovskii A M and Makarov D E 2021 On distributions of barrier crossing times as observed in single-molecule studies of biomolecules *Biophys. Rep.* **1** 100029
[22] Chung H S and Eaton W A 2018 Protein folding transition path times from single molecule FRET *Curr. Opin. Struct. Biol.* **48** 30–39
[23] Chung H S and Gopich I V 2014 Fast single-molecule FRET spectroscopy: theory and experiment *Phys. Chem. Chem. Phys.* **16** 18644–57
[24] Bowman G R, Pande V S and Noé F 2013 *An Introduction to Markov State Models and Their Application to Long Timescale Molecular Simulation* (Springer Science & Business Media)
[25] Meng Y, Shukla D, Pande V S and Roux B 2016 Transition path theory analysis of c-Src kinase activation *Proc. Natl Acad. Sci. USA* **113** 9193–8
[26] Bolhuis P G, Chandler D, Dellago C and Geissler P L 2002 Transition path sampling: throwing ropes over rough mountain passes, in the dark *Annu. Rev. Phys. Chem.* **53** 291–318
[27] Rubino G and Tuffin B 2009 *Rare Event Simulation Using Monte Carlo Methods* (Wiley)
[28] Van Erp T S and Bolhuis P G 2005 Elaborating transition interface sampling methods *J. Comput. Phys.* **205** 157–81
[29] Torrie G M and Valleau J P 1977 Nonphysical sampling distributions in Monte Carlo free-energy estimation: umbrella sampling *J. Comput. Phys.* **23** 187–99
[30] E W, Ren W and Vanden-Eijnden E 2002 String method for the study of rare events *Phys. Rev.* B **66** 052301
[31] Allen R J, Frenkel D and Ten Wolde P R 2006 Forward flux sampling-type schemes for simulating rare events: efficiency analysis *J. Chem. Phys.* **124** 194111
[32] Reiner M M, Bachmair B, Tiefenbacher M X, Mai S, González L, Marquetand P and Dellago C 2023 Nonadiabatic forward flux sampling for excited-state rare events *J. Chem. Theory Comput.* **19** 1657–71
[33] Zhu Y, Tang Y and Kim C 2023 Learning stochastic dynamics with statistics-informed neural network *J. Comput. Phys.* **474** 111819
[34] Harlim J, Jiang S, Liang S and Yang H 2021 Machine learning for prediction with missing dynamics *J. Comput. Phys.* **428** 109922
[35] Chen Y and Xiu D 2024 Learning stochastic dynamical system via flow map operator *J. Comput. Phys.* **508** 112984
[36] Fang C, Lu Y, Gao T and Duan J 2023 Reservoir computing with error correction: long-term behaviors of stochastic dynamical systems *Physica* D **456** 133919
[37] Jung H, Covino R, Arjun A, Leitold C, Dellago C, Bolhuis P G and Hummer G 2023 Machine-guided path sampling to discover mechanisms of molecular self-organization *Nat. Comput. Sci.* **3** 334–45
[38] Kim W K and Netz R R 2015 The mean shape of transition and first-passage paths *J. Chem. Phys.* **143** 224108
[39] Risken H 1989 *The Fokker–Planck Equation: Method of Solution and Application* (Springer)

[40] Berezhkovskii A M, Dagdug L and Bezrukov S M 2017 Mean direct-transit and looping times as functions of the potential shape *J. Phys. Chem.* B **121** 5455–60
[41] Berezhkovskii A M, Dagdug L and Bezrukov S M 2020 Peculiarities of the mean transition path time dependence on the barrier height in entropy potentials *J. Phys. Chem.* B **124** 2305–10
[42] Li H, Xu Y, Li Y and Metzler R 2020 Transition path dynamics across rough inverted parabolic potential barrier *Eur. Phys. J. Plus* **135** 1–22
[43] Berezhkovskii A M, Hummer G and Bezrukov S M 2006 Identity of distributions of direct uphill and downhill translocation times for particles traversing membrane channels *Phys. Rev. Lett.* **97** 020601
[44] Gladrow J, Ribezzi-Crivellari M, Ritort F and Keyser U F 2019 Experimental evidence of symmetry breaking of transition-path times *Nat. Commun.* **10** 55
[45] Janakiraman D 2018 Transition path time distributions for Lévy flights *J. Phys. A: Math. Theor.* **51** 285001
[46] Li H, Xu Y, Metzler R and Kurths J 2020 Transition path properties for one-dimensional systems driven by Poisson white noise *Chaos Solitons Fractals* **141** 110293
[47] Berezhkovskii A M, Bezrukov S M and Makarov D E 2021 Localized potential well vs binding site: mapping solute dynamics in a membrane channel onto one-dimensional description *J. Chem. Phys.* **154** 111101
[48] Zwanzig R 1973 Nonlinear generalized Langevin equations *J. Stat. Phys.* **9** 215–20
[49] Lei H, Baker N A and Li X 2016 Data-driven parameterization of the generalized Langevin equation *Proc. Natl Acad. Sci. USA* **113** 14183–8
[50] Ślezak J, Burnecki K and Metzler R 2019 Random coefficient autoregressive processes describe Brownian yet non-Gaussian diffusion in heterogeneous systems *New J. Phys.* **21** 073056
[51] Min W, Luo G, Cherayil B J, Kou S C and Xie X S 2005 Observation of a power-law memory kernel for fluctuations within a single protein molecule *Phys. Rev. Lett.* **94** 198302
[52] Sandev T, Chechkin A, Kantz H and Metzler R 2015 Diffusion and Fokker–Planck-Smoluchowski equations with generalized memory kernel *Fractional Calculus Appl. Anal.* **18** 1006–38
[53] Lin L, He M and Wang H 2022 Collective resonant behaviors in two coupled fluctuating-mass oscillators with tempered Mittag-Leffler memory kernel *Chaos Solitons Fractals* **154** 111641
[54] Baczewski A D and Bond S D 2013 Numerical integration of the extended variable generalized Langevin equation with a positive Prony representable memory kernel *J. Chem. Phys.* **139** 044107
[55] Duong M H and Shang X 2022 Accurate and robust splitting methods for the generalized Langevin equation with a positive Prony series memory kernel *J. Comput. Phys.* **464** 111332
[56] Bao J and Zhuo Y 2003 Ballistic diffusion induced by a thermal broadband noise *Phys. Rev. Lett.* **91** 138104
[57] Ayaz C, Scalfi L, Dalton B A and Netz R R 2022 Generalized Langevin equation with a nonlinear potential of mean force and nonlinear memory friction from a hybrid projection scheme *Phys. Rev.* E **105** 054138
[58] Chaudhury S and Cherayil B J 2006 Complex chemical kinetics in single enzyme molecules: Kramers' model with fractional Gaussian noise *J. Chem. Phys.* **125** 024904
[59] Xu P and Jin Y 2020 Coherence and Stochastic resonance in a second-order asymmetric tri-stable system with memory effects *Chaos Solitons Fractals* **138** 109857
[60] Metzler R 2020 Superstatistics and non-Gaussian diffusion *Eur. Phys. J. Spec. Top.* **229** 711–28
[61] Ferreira R M S 2022 From generalized Langevin stochastic dynamics to anomalous diffusion *Phys. Rev.* E **106** 054157
[62] Chen W, Greiner C and Xu Z 2023 Persistent nonequilibrium effects in generalized Langevin dynamics of nonrelativistic and relativistic particles *Phys. Rev.* E **107** 064131
[63] Plyukhin A V 2023 Nonergodic Brownian oscillator: high-frequency response *Phys. Rev.* E **107** 044107
[64] Sharma S, Singh V and Biswas P 2021 Effect of ligand binding on riboswitch folding: theory and simulations *J. Chem. Phys.* **154** 185101
[65] Ayaz C , Tepper L, Brünig F N, Kappler J, Daldrop J O and Netz R R 2021 Non-Markovian modeling of protein folding *Proc. Natl Acad. Sci. USA* **118** e2023856118
[66] Satija R, Das A and Makarov D E 2017 Transition path times reveal memory effects and anomalous diffusion in the dynamics of protein folding *J. Chem. Phys.* **147** 152707
[67] Singh D, Mondal K and Chaudhury S 2021 Effect of memory and inertial contribution on transition-time distributions: theory and simulations *J. Phys. Chem.* B **125** 4536–45

[68] Carlon E, Orland H, Sakaue T and Vanderzande C 2018 Effect of memory and active forces on transition path time distributions *J. Phys. Chem.* B **122** 11186–94
[69] Medina E, Satija R and Makarov D E 2018 Transition path times in non-Markovian activated rate processes *J. Phys. Chem.* B **122** 11400–13
[70] Kubo R, Toda M and Hashitsume N 1985 *Statistical Physics II: Nonequilibrium Statistical Mechanics* (Springer)
[71] Zwanzig R 2001 *Nonequilibrium Statistical Mechanics* (Oxford University Press)
[72] Yang H, Luo G B, Karnchanaphanurach P, Louie T M, Rech I, Cova S, Xun L and Xie X S 2003 Protein conformational dynamics probed by single-molecule electron transfer *Science* **302** 262
[73] Palyulin V V, Ala-Nissila T and Metzler R 2014 Polymer translocation: the first two decades and the recent diversification *Soft Matter* **10** 9016
[74] Doerries T J, Loos S A M and Klapp S H L 2021 Correlation functions of non-Markovian systems out of equilibrium: analytical expressions beyond single-exponential memory *J. Stat. Mech.* 033202
[75] Vroylandt H, Goudenège L, Monmarché P, Pietrucci F and Rotenberg B 2022 Likelihood-based non-Markovian models from molecular dynamics *Proc. Natl Acad. Sci. USA* **119** e2117586119
[76] Kappler J, Hinrichsen V B and Netz R R 2019 Non-Markovian barrier crossing with two-time-scale memory is dominated by the faster memory component *Eur. Phys. J.* E **42** 119
[77] Okuyama S and Oxtoby D W 1986 The generalized Smoluchowski equation and non-Markovian dynamics *J. Chem. Phys.* **84** 5824–9
[78] Bicout D J and Szabo A 1998 Electron transfer reaction dynamics in non-Debye solvents *J. Chem. Phys.* **109** 2325–38
[79] Goychuk I 2012 Viscoelastic subdiffusion: generalized Langevin equation approach *Adv. Chem. Phys.* **150** 187
[80] Hänggi P and Thomas H 1982 Stochastic processes: time evolution, symmetries and linear response *Phys. Rep.* **88** 207
[81] Bao J 2004 Numerical integration of a non-Markovian Langevin equation with a thermal band-passing noise *J. Stat. Phys.* **114** 503–13